Voltage-Controlled Bistable Thermal Conductivity in Suspended Ferroelectric Thin-Film Membranes

Brian M. Foley,[†,∇] Margeaux Wallace,[‡,°] John T. Gaskins,[†] Elizabeth A. Paisley,[§]
Raegan L. Johnson-Wilke,[§] Jong-Woo Kim,[∥] Philip J. Ryan,[∥] Susan Trolier-McKinstry,[‡]
Patrick E. Hopkins,[*,†,⊥,#] and Jon F. Ihlefeld[*,§,⊥,¶]

[†]Department of Mechanical and Aerospace Engineering, [⊥]Department of Materials Science and Engineering, [#]Department of Physics, and [¶]Charles L. Brown Department of Electrical and Computer Engineering, University of Virginia, Charlottesville, Virginia 22904, United States

[‡]Department of Materials Science and Engineering and Materials Research Institute, The Pennsylvania State University, University Park, Pennsylvania 16802, United States

[§]Sandia National Laboratories, Albuquerque, New Mexico 87185, United States

[∥]Advanced Photon Source, Argonne National Laboratory, Lemont, Illinois 60439, United States

ABSTRACT: Ferroelastic domain walls in ferroelectric materials possess two properties that are known to affect phonon transport: a change in crystallographic orientation and a lattice strain. Changing populations and spacing of nanoscale-spaced ferroelastic domain walls lead to the manipulation of phonon-scattering rates, enabling the control of thermal conduction at ambient temperatures. In the present work, lead zirconate titanate (PZT) thin-film membrane structures were fabricated to reduce mechanical clamping to the substrate and enable a subsequent increase in the ferroelastic domain wall mobility. Under application of an electric field, the thermal conductivity of PZT increases abruptly at ∼100 kV/cm by ∼13% owing to a reduction in the number of phonon-scattering domain walls in the thermal conduction path. The thermal conductivity modulation is rapid, repeatable, and discrete, resulting in a bistable state or a "digital" modulation scheme. The modulation of thermal conductivity due to changes in domain wall configuration is supported by polarization-field, mechanical stiffness, and in situ microdiffraction experiments. This work opens a path toward a new means to control phonons and phonon-mediated energy in a digital manner at room temperature using only an electric field.

KEYWORDS: phonons, domains, tunable, ferroelectric, time-domain thermoreflectance, nanodomain
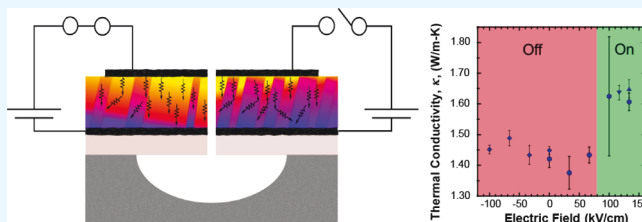
1. INTRODUCTION

Deterministic control of phonon transport in the solid state represents a new paradigm of energy regulation. If such control could be realized, it would not only enable active thermal energy regulation but could also impact electronic and optical energies by controlling phonon-coupled particles and waves, such as polarons and polaritons. Further, one could realize technologies where phonons are the energy form being manipulated, thus enabling a relatively new field of phononics. Although multiform energy control and phononics may enable technologies of the future, immediate impacts could be realized by an ability to regulate the primary signature of phonons: thermal transport. For example, minimizing thermal transport is necessary to achieve high-value thermoelectric responses for both cooling and energy harvesting;[1] maximizing heat transport in semiconductor-based electronic devices is necessary to maintain device efficiency and prevent degradation;[2] and maintaining thermal isolation is required for infrared sensors and detectors to minimize cross talk and maximize signal-to-noise ratios,[3] among many other applications. Most

means to control phonon and, subsequently, thermal transport are passive in nature: a material's thermal conductivity is fixed at a particular temperature, and temperature gradients are utilized to modulate the heat flux. The ability to alter a material's thermal conductivity on demand would permit the development of thermal switches or regulators with a new degree of control. For example, much in the same way that field effects can be used to alter electronic conduction through a semiconductor, a material with actively tunable thermal conductivity could be used to modulate thermal transport. To date, however, the means to realize such control over phonons and thermal energy are extremely limited.

In solid-state materials, abrupt thermal conductivity changes are most commonly observed by passing through phase transitions where the phases on each side of the transition have differing thermal responses. Large differences in thermal

conduction have been observed using this effect in carbon nanotube/hexadecane composites[4] and graphite/hexadecane composites,[5] where the liquid and solid phases have vastly different properties. Likewise, transitions from an insulating phase to an electrically conducting phase can impart large changes in thermal conductivity by introducing large concentrations of heat-carrying electronic carriers. This effect has been demonstrated in insulator−metal transition materials, such as VO_2, where changes in thermal conductivity up to 60% have been measured at the phase transition.[6] These approaches to thermal conduction control, however, rely on changing the parameter that one wishes to control—thermal energy—to be achieved.

Other nonthermal forms of control have been demonstrated to affect thermal conductivity in specific systems, including electric and magnetic field effects. For example, modulating charge carriers in semiconducting InAs nanowires with electric and magnetic fields affected thermal conduction at cryogenic temperatures.[7] Magnetic fields have been shown to alter the population of magnons in magnetic nanowires, enabling the control of thermal conductivity across a broad temperature range.[8] The inherent thinness of nanowires, however, limits the amount of thermal energy that can be manipulated by such an approach. Active composition changes have also been explored, whereby modifying the composition of $LiCoO_2$ via intercalation/deintercalation of lithium results in ~30% changes in thermal conductivity.[9] This approach requires a battery cell to provide and remove lithium and has a response time limited to the diffusivity of lithium in the $LiCoO_2$ lattice.

An alternative approach to active thermal control would be to utilize reconfigurable phonon-scattering interfaces. This can be achieved, for example, by the use of ferroelastic domain boundaries in ferroelectric materials. By altering the numbers of domain walls present within the ferroelectric material, the thermal conductivity can be modified. This has been shown to produce active regulation at cryogenic temperatures in $BaTiO_3$[10] and KH_2PO_4[11,12] single crystals. In the former work, a repeatable increase of thermal conductivity was shown by simply applying an electric field across the sample and thereby reducing the number of domain walls and the number of phonon-scattering interfaces. The response time was hypothesized to be as fast as the domain-switching time in a ferroelectric material, which can be in the regime of nanoseconds.[13] Thin films provide an advantage over most single-crystal and bulk ceramic ferroelectric materials in that the scaling of crystal dimensions to smaller sizes results in the reduction of domain wall spacing,[14] coupled with a decrease in the required voltage for modulation. By decreasing the spacing of the walls to a magnitude similar to the mean-free paths of heat-carrying phonons, which would be expected to be 10−100 s of nanometers at room temperature in a ferroelectric film,[15] modulation of thermal conductivity can be realized at noncryogenic temperatures. This was demonstrated passively at room temperature in 30 nm thick $BiFeO_3$ thin films where films with differing populations of 71° domain walls exhibited differences in thermal conductivity up to 400 K.[16] Active modulation was shown at room temperature in 200 nm thick bilayer lead zirconate titanate (PZT) thin films where an electric field-dependent, varying population of closely spaced 90° domain walls in a tetragonally distorted PZT layer produced thermal conduction tuning.[17]

To achieve thermal conductivity tuning using domain wall reconfiguration, the populations of these walls must be modulated by an external stimulus. However, mechanical clamping to the substrate is known to restrict ferroelastic domain wall motion in thin films and therefore must be reduced in order to realize significant domain structure changes.[18,19] There are several means to achieve this: (1) selected removal of the underlying substrate,[20,21] (2) reducing the lateral dimensions of the ferroelectric film,[19,22,23] (3) utilizing mechanically compliant layers such as ferroelectric bilayers[24] or compliant substrates,[25] (4) preparing thick (several micron) ferroelectric layers,[26] or (5) preparing films with large lateral grain sizes.[26] It has previously been demonstrated that the bilayers enable ferroelastic domain wall motion and alteration of thermal conductivity.[17] For those largely clamped films, however, the material response to an increased electric field was an *increase* in the numbers of domain walls and a subsequent *reduction* in thermal conductivity. Furthermore, a nearly linear response between the tuning of thermal conductivity and the applied electric field was observed, that is, an "analog" or continuously variable modulation response. It was believed that the clamping of the thin film to a relatively thick silicon wafer imposed a mechanical boundary condition that limited domain growth and resulted in an increasing domain boundary density under electric fields, which was consistent with the work on other bilayer films[24,27,28] and large grained tetragonal PZT films.[29] In the present work, it is shown that declamping from the substrate via selected removal of silicon below a PZT film enables an increase in thermal conductivity by up to 13% at room temperature with an applied electric field. The thermal conductivity increase occurs because the domain wall density decreases owing to the ability of domains to grow with reduced mechanical clamping. In this case, the increase occurs abruptly and is discrete in nature, assuming one of the two possible conductivity states. The thermal conductivity change is correlated with the electric fields at which polarization reversal occurs, mechanical stiffness of the structure changes, and domain population changes are observed with microdiffraction.

2. METHODS

2.1. Materials and Membrane Device Fabrication. PZT thin films of composition $PbZr_{0.3}Ti_{0.7}O_3$ were prepared on platinized silicon substrates (100 nm Pt/40 nm ZnO/400 nm SiO_2/silicon) via chemical solution deposition.[30] Chemical solutions were prepared from an inverted mixing order chemistry[31] using lead (IV) acetate (Sigma-Aldrich), titanium isopropoxide, zirconium butoxide (80 wt % in 1-butanol), methanol, and acetic acid. A 0.35 M solution was prepared and used for the $PbZr_{0.3}Ti_{0.7}O_3$ composition and was batched with 10% excess lead acetate to compensate for lead loss to the atmosphere during crystallization. The films were spin-cast at 4000 rpm for 30 s, followed by a 350 °C hot-plate pyrolysis. After three coating and pyrolysis steps, the film was annealed at 700 °C for 10 min in a preheated furnace to crystallize into the perovskite phase. The coating, pyrolysis, and crystallization anneal steps were repeated three times to prepare a 600 nm thick film. To promote a (100)/(001) crystallographic texture in the PZT films, a thin seed layer of $PbTiO_3$ was deposited prior to the PZT.[32,33] The 0.05 M $PbTiO_3$ solution with 10% excess lead acetate was spin-cast at 6000 rpm for 30 s, followed by a 350 °C hot-plate pyrolysis and a 700 °C 10 min crystallization anneal.

Substrate clamping was reduced by undercutting the silicon substrate in diaphragm structures.[20] Platinum top electrodes, 100 nm thick, were prepared via photolithography, sputter deposition, and lift-off. A second photolithography step was used to define an array of 5 μm diameter holes. Reactive ion etching was performed to provide an opening to the underlying silicon substrate. Finally, a XeF_2 etch
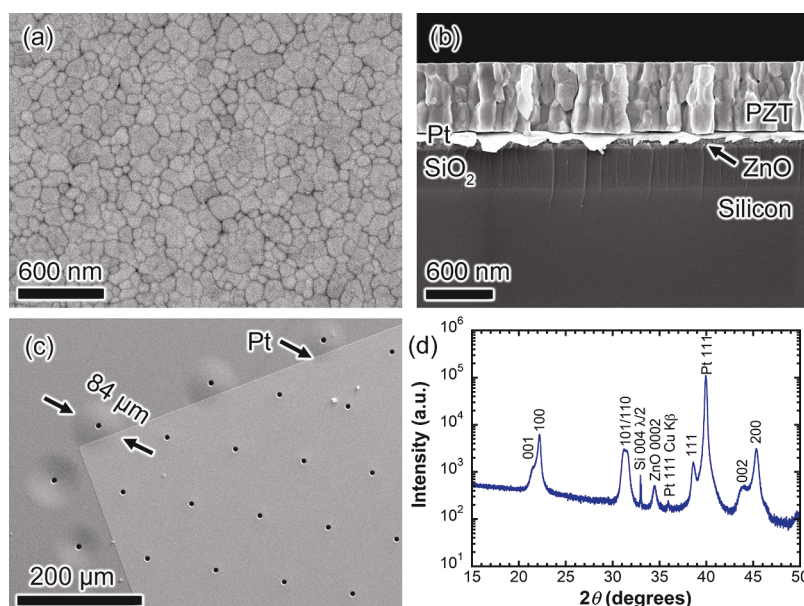
Figure 1. Scanning electron microscopy images of the 600 nm thick PZT film prepared on a Pt/ZnO/SiO₂/Si substrate: (a) plan-view image and (b) cross section displaying a dense columnar grain morphology and (c) plan-view image of the membrane array. The holes in the membranes were formed by reactive ion etching and the released regions by a XeF₂ etch of the underlying silicon. (d) X-ray diffraction pattern of the film.

was performed to selectively remove silicon to form cavities underneath a Pt/PZT/Pt/ZnO/SiO₂ diaphragm. The resulting membranes were approximately 84 μm in diameter. The details of the etch chemistry and diaphragm formation procedure can be found elsewhere.[21]

2.2. Characterization. To measure the thermal transport properties of the strain-released PZT films under applied electric fields, an electrical probe station was integrated into a time-domain thermoreflectance (TDTR) system. TDTR is an optical pump–probe measurement technique, which utilizes subpicosecond ($<10^{-12}$ s) laser pulses to monitor energy transport within nanostructures occurring over time scales from single picoseconds to multiple nanoseconds. The experiment is based on splitting the femtosecond pulse train of 800 nm light emanating from an optical oscillator (Spectra-Physics Tsunami) into two new beams. One beam serves as the "pump" beam and provides a heating event at the sample surface and the other as the "probe" beam that arrives at a later time and measures the temperature of the sample surface via changes in its thermoreflectance coefficient (dR/dT). The diameters of the focused pump and probe beams at the surface of the sample were determined using a scanning-slip beam profiler and measured to be 26 and 24 μm, respectively. The pump beam passes through an electro-optic modulator, where the train of pulses is amplitude-modulated at 3.74 MHz, and the change in the probe reflectivity as a function of pump–probe delay time is recorded via a lock-in amplifier triggered to the pump modulation frequency. By fitting this decay profile to a variety of models depending on the time scale of interest, a wide array of physical properties related to the sample of interest can be deduced.[34−36]

Thermal conductivity was measured using the top platinum pad as both a TDTR transducer and an electrical contact with which to apply dc fields across the membranes. An optical microscope attached to the TDTR system was used to align the measurement region to be on a membrane region of the PZT film, focused between the clamped edge and the center hole of the membrane, and TDTR experiments were then conducted as different dc electric fields (E) were applied across the Pt/PZT/Pt structures using a Keysight E4980A LCR meter. The location of the laser spot on the membrane remained fixed for all of the thermal measurements at various electric field magnitudes, thereby producing an assessment of the change in thermal conductivity under that specific sampled volume of PZT. By doing so, various factors such as local micro/domain structure of the PZT,

platinum film thickness, beam overlap, spot sizes, and focal position can be treated as common to and constant throughout all electrical bias conditions. As a result, many of the dominant sources of uncertainty commonly associated with TDTR are minimized, enabling highlighting of the change in thermal conductivity associated with the applied bias. The remaining sources of uncertainty in this experimental design are the phase and/or $1/f$ noise, as well as the scan-to-scan repeatability of the TDTR data acquisition process as a whole. In general, these sources of uncertainty are expected to be much smaller than the aforementioned elements that were minimized. Measurement uncertainty related to the influence of noise and the scan-to-scan repeatability of TDTR were accounted for by taking three scans in succession at each bias field condition.

The temporal TDTR measurements (where the bias across the membrane was cycled with time) were performed with the probe delay relative to the pump pulse fixed at 500 ps to minimize the sensitivity of the thermal model to changes in the thermal boundary conductance between the top platinum electrode and PZT, while allowing nearly full diffusion of deposited layer energy through the platinum electrode (i.e., reducing the sensitivity to the thermal conductivity of the platinum). The thermoreflectance of the platinum electrode is directly related to the temperature of the metal. Therefore, for a fixed power deposited on the device by the laser and a resulting heat flux through the sample structure, any changes in the temperature of the top electrode are indicative of changes in the thermal resistance of the multilayer structure beneath it when bias is applied or removed. This pump–probe delay time allowed for the real-time observation of the dynamic switching of the thermal conductivity of the PZT membrane.

Polarization versus electric field hysteresis data were collected at 100 Hz with a Radiant Technologies Multiferroic Workstation. Voltages were applied to the membrane during TDTR, nano-indentation, and X-ray microdiffraction using an Agilent 4284 or a Keysight E4980 LCR meter. Use of an LCR meter enabled the "health" of the device to be monitored with the loss tangent during the test to ensure that the devices were not degrading electrically. Scanning electron microscopy was performed with Zeiss Supra 55VP instruments operating in an in-lens imaging mode with a 3 kV accelerating voltage and a backscatter mode with a 20 kV accelerating voltage (plan-view microstructure). The electrode areas were calculated from optical micrographs using image analysis software (ImageJ). An X-ray diffraction pattern to assess crystallographic
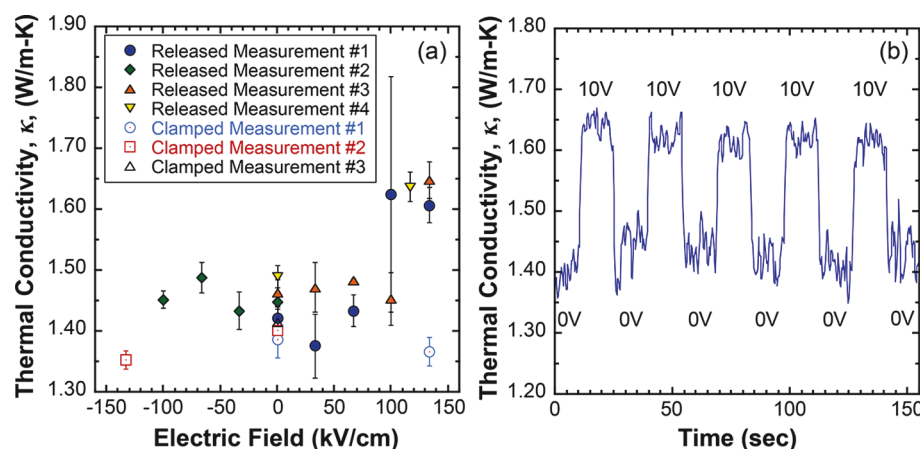
Figure 2. (a) Room-temperature thermal conductivity of PZT in the membrane device (closed symbols) and in the clamped region (open symbols) as a function of applied dc field. (b) Room-temperature thermal conductivity of PZT in the membrane device as a function of time as a dc voltage is modulated across the structure.

orientation and phase assemblage was collected with a PANalytical Empyrean instrument with Cu Kα radiation in a Bragg–Brentano geometry.

The membrane stiffness measurements were performed via nanoindentation using an Agilent Technologies DCM II instrument and a method described elsewhere.[37,38] A 50 μm radius spherical tip was used to apply a point load, which in this case specifically refers to the loading condition, in the center of the membrane. Calculation of the contact radius between a sphere and flat elastic body reveals that the contact radius grows to greater than 10 microns in less than 100 nm of displacement into the body, so the indenter is assumed to apply an evenly distributed load to the outside edge of the etch hole, which is approximated as a point load in the middle of the released membrane. Several membranes were tested to obtain a baseline film deflection in the unpoled state and examine the repeatability on structures in the array. After confirmation of nearly identical mechanical behavior between membranes in adjacent array lines, voltage sweeps were performed up to 5 V in 2.5 V increments, followed by 1 V increments up to 10 V on an untested membrane to examine the effect of voltage on the stiffness of the membrane. The stiffness of the membrane under an applied point load, P, assuming no prestrain, is defined from Komaragiri et al. as[39]

$$\frac{P}{w(0)} = \frac{4\pi}{3(1 - \nu^2)}\left(\frac{Eh^3}{a^2}\right) \tag{1}$$

where $w(0)$ is the center span deflection, a is the membrane radius, ν is the average Poisson's ratio, E is the average Young's modulus, and h is the thickness of the entire membrane. Using literature values,[40–43] we calculate an average Poisson's ratio of 0.31 and an average Young's modulus of 94 GPa by taking a thickness-weighted average of the properties of each layer of the membrane. Using the above equation, we then calculate a stiffness of 470 N/m for the membrane.

Synchrotron X-ray diffraction experiments were performed at the Advanced Photon Source at Argonne National Laboratory, beamline 6ID-B. An X-ray beam on a sample footprint size of 5 μm width and 23 μm length and an energy of 16.2 keV were used to enable local probing of the released diaphragm structures. The intensity of the 002 and 200 diffraction peaks was recorded as a function of applied dc field using a Keithley 2410, and the PZT film was monitored using an Agilent 4284 LCR meter. Data were obtained by aligning to the maximum intensity of the PZT 002 and 200 positions and measuring intensity, while the dc bias was varied by 0.25 V steps within a −10 to 10 V range. The diffraction intensity was recorded at each step. For all locations, PZT c- and a-domain intensities were normalized to the beam current and platinum 111 reflection reference to account for changes in beam intensity over measurement time.

3. RESULTS AND DISCUSSION

Figure 1a,b shows plan-view and cross-sectional scanning electron micrographs, respectively, of the PZT thin film. A dense, columnar grain morphology is evident with lateral grain sizes on the order of 100 nm and a film thickness of approximately 600 nm. The as-prepared membrane structure is shown in the plan-view electron microscopy image in Figure 1c. A row of the milled hole array lies outside of the platinum top electrode. In this region, the size of the membrane structure is evident by the slight deflection of the film surface owing to strain relief. The width of the deflected area, and therefore the diameter of the membranes, is approximately 84 μm. Figure 1d shows an X-ray diffraction pattern of the film. Only peaks associated with the PZT film and materials in the substrate stack are observed, indicating phase purity. The greater intensity of the 100 peak compared to that of 101/110 and 111 peaks indicates that the PbTiO$_3$ seed layer aided in enhancing the (100)/(001) crystallographic orientation.

Figure 2a shows the measured thermal conductivity of the suspended PZT membrane (closed data points) under applied electric fields. Several separate sweeps, where the magnitude of the applied dc field was varied, are presented in the order of the sequence in which they were conducted. Starting with the general trends between the measurement sequences, it is observed that the thermal conductivity remains unchanged for electric fields 0 ≤ E < 100 kV/cm with values of ~1.42 W/m K, increases abruptly at around 100 kV/cm, and maintains a higher value of thermal conductivity of ~1.61 W/m K for fields ≥100 kV/cm. At the onset of the thermal conductivity change (100 kV/cm), this previously unpoled structure exhibited noticeable instability over the time scale of the TDTR scans (three scans, 2–3 min each), indicating that a dynamic process was taking place within the device. The large error bars for the 100 kV/cm data point are indicative of this instability. The change in thermal conductivity between the low-field (<100 kV/cm) and high-field (>100 kV/cm) conditions is an approximate 13% increase. Following the first exposure to high fields (released measurement #1), the bias was removed and the thermal conductivity returned to a value of 1.45 ± 0.01 W/m K, which is similar to, but slightly higher than, the previously unpoled value of 1.42 ± 0.03 W/m K, suggesting a reversibility of the thermal conduction properties. The reversibility is likely due to the restoring forces associated

with the membrane tension in the released structure. Upon driving the device with the opposite polarity (released measurement #2), no change in thermal conductivity was observed for fields of −100 kV/cm with the thermal conductivity value constant at approximately 1.44 W/m K. In this polarity, the dielectric loss tangent increased for fields above −100 kV/cm; the applied field was restricted to prevent device damage. Releasing the dc electric field and returning to zero bias resulted in a slight increase in thermal conductivity to 1.46 ± 0.02 W/m K and again driving a positive bias across the device (released measurements #3 and #4) revealed a sudden increase in thermal conductivity to ∼1.6 W/m K for fields greater than 100 kV/cm. These results demonstrate repeatability of the discrete thermal conductivity regulation.

To provide an assessment of the speed with which this change in thermal conductivity occurs, the thermoreflectance of the platinum top electrode on the membrane was monitored in real time as dc bias was applied and removed. The thermal conductivity of PZT in the membrane structure could then be calculated with the results shown in Figure 2b. As the bias voltage applied across the structure was cycled between 0 and 10 V (167 kV/cm), changes in thermal conductivity occurring over a subsecond time scale are observed with zero bias values of approximately 1.44 W/m K increasing to 1.62 W/m K when the 167 kV/cm field was applied. Although the response is clearly subsecond, in actuality, the switching most likely happens over much shorter time scales, possibly as short as 40 ns,[44] as the absolute speed of detection is limited by the 300 ms time constant of the lock-in amplifier used in the TDTR measurement.

To verify that the domain structure changes are responsible for the observed behavior, a control experiment was performed by measuring a clamped region (i.e., measuring on a metal trace away from the membrane) on the same electrode with and without electric fields applied. These results are shown as the open data points in Figure 2a. As opposed to the dramatic, rapid change in thermal conductivity with field that was measured on the membrane, virtually no change was observed for the clamped region. It is observed that the zero bias values change from 1.38 ± 0.03 W/m K on the first measurement to 1.41 ± 0.03 W/m K after subsequent applications of 133 and −133 kV/cm, respectively. At 133 kV/cm, the thermal conductivity of the clamped region was 1.37 ± 0.02 W/m K and under −133 kV/cm was 1.35 ± 0.02 W/m K. These data, showing no change in thermal conductivity, suggest that the ferroelastic domain wall motion in the clamped region is hindered and that the domain wall spacing and/or density of domain walls remains relatively constant, as has been shown elsewhere.[21] The differences in thermal conductivity response to the electric field between the membrane structure and the clamped region strongly indicate that the ferroelastic domain boundary populations are changing, leading to variations in phonon scattering. To confirm the mechanisms of the change, additional experiments were performed to investigate the electrical and mechanical properties. Figure 3 shows room-temperature-nested polarization hysteresis loops for the Pt/PZT/Pt device. Note that this measurement samples the ensemble clamped and suspended membrane response because the membranes constitute a fraction of the overall electrode area. Regardless, it is clear that the coercive fields of the structure are approximately −130 and 110 kV/cm. The asymmetry is indicative of a degree of imprint in these films, which may result due to the reactive ion etching used to
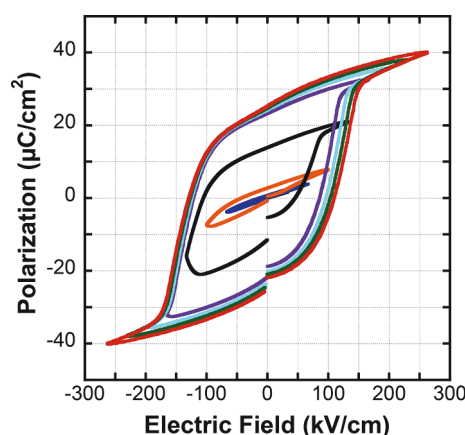

Figure 3. Polarization vs dc electric field, $P(E)$, response of a PZT film comprising clamped and membrane regions.

prepare the membrane structures.[45] The 110 kV/cm coercive field value is similar to the fields at which the sudden thermal conductivity increase is observed in the membrane structure (100 kV/cm) and suggests that the onset of the large thermal conductivity change with electric field is associated with the field required for polarization reversal. As polarization reversal requires nucleation and growth of domains, this is a strong indicator that the field-induced increase in thermal conductivity at 100 kV/cm in the membrane is due to domain structure changes. It should be noted that the coercive field measured from the polarization-field measurements is slightly higher than the field required for the thermal conductivity change. Substrate clamping is known to result in increased coercive fields.[46] Because the $P(E)$ response shown here is a composite response of clamped and unclamped regions, a higher coercivity of the clamped regions may lead to higher measured overall values. Additionally, it is known that measurement frequency affects coercive field measurements with fast rates (higher measurement frequencies), resulting in higher reported values.[47] The 100 Hz measurement frequency of the polarization response compared to the dc measurement of thermal conductivity may also, in part, be responsible for the difference in measured coercive field and the onset of thermal conductivity switching.

To gather property information on an individual membrane, local stiffness measurements were performed using a nano-indenter with and without fields applied. Starting from an unpoled condition and applying an increasing dc field will result in poling of the ferroelectric and domain reconfiguring. It was anticipated that the domain motion, which constitutes an extrinsic piezoelectric effect, and the intrinsic piezoelectric effect upon poling will affect the stiffness of the membrane.[48] The nanoindenter tip was located in the center of an unpoled membrane, and its stiffness was measured at zero bias and while dc electric fields are applied. Figure 4 shows the electric field dependence of membrane stiffness. It is observed that the stiffness remains constant at approximately 500 N/m until an electric field of 100 kV/cm, at which point the stiffness of the membrane increases. At an applied dc field of 167 kV/cm, the stiffness reaches ∼850 N/m. Upon reducing the electric field to 0 kV/cm, the membrane stiffness does not fully recover to its original value but decreases to 625 N/m. While under the application of a field, the dc bias constrains the domain wall motion[49] against the force applied by the nanoindenter and increases the membrane stiffness. The onset of membrane
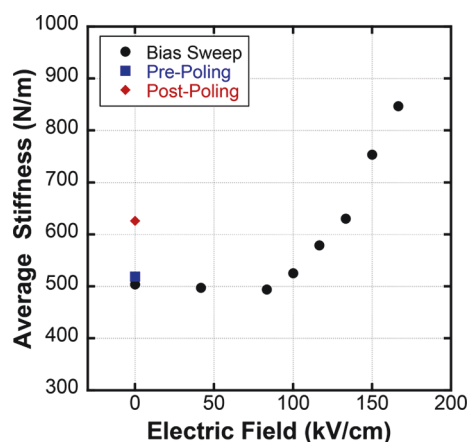
Figure 4. Membrane stiffness before (prepoling), during application of a dc electric field, and after application of a dc electric field (postpoling).

stiffness increase at 100 kV/cm correlates well with the coercive field from the polarization field measurements and the onset of thermal conductivity increase and provides additional evidence that the bias at which ferroelastic domain wall motion and domain growth occur in these membrane structures is approximately 100 kV/cm.

As a final local probe of the domain structure, synchrotron X-ray microdiffraction measurements were performed on the membrane structures. Figure 5 plots the normalized intensity
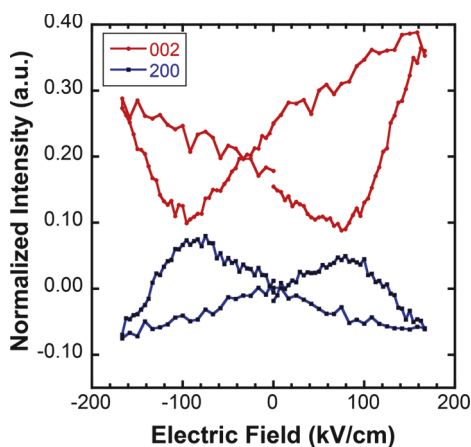

Figure 5. Normalized intensity of 002 and 200 diffraction peaks of PZT in a membrane device as measured by synchrotron X-ray microdiffraction as a function of applied field.

of the 200 and 002 diffraction peaks of PZT as a function of applied dc electric field. The data shown are for a membrane that is initially in a negatively poled state. Focusing on the 002 diffraction peak, starting from zero bias, it is observed that the intensity decreases and reaches a minimum at approximately 75 kV/cm, at which point the diffraction intensity increases roughly linearly. Reversing the field results in a nearly linear decrease in intensity, reaching a minimum at approximately −105 kV/cm before increasing again. On the basis of the disparity between the fields of intensity minima, the imprint effects that were observed in the polarization response are clearly present in the microdiffraction data. Between 75 and 167 kV/cm, the 002 peak intensity increases rapidly. Because both peak intensities are directly related to domain volume

fractions, changes in their relative intensities indicate changes in ferroelastic domain wall populations. The increase in 002 peak intensity demonstrates an increase in the volume fraction of (00l)-oriented domains—those domains that are best aligned with the electric field vector—whereas the concomitant decrease in 200 peak intensity is consistent with ferroelastic switching. The 75 kV/cm field represents the initiation of domain growth and compares well with the polarization measurements (note that the onset of steep polarization change in the polarization measurement is ∼75 kV/cm, whereas the field representing zero polarization is ∼110 kV/cm). The diffraction data, combined with the polarization-field and mechanical stiffness measurements, which all show nearly the same electric field for a property change—peak intensity increase, coercive field, and stiffness increases, respectively—provide strong evidence that the ferroelastic domain wall motion is responsible for the observed thermal conductivity discontinuity. That the thermal conductivity *increased* when the electric field was applied suggests that the domains that were most well aligned with the electric field grew at the expense of those that were not well aligned. In this process, the spacing between the domain walls increased, the number of ferroelastic domain walls decreased, and, consequently, the number of phonon-scattering interfaces within the film in the membrane region decreased. The result was an abrupt increase in the thermal conductivity. This result is consistent with the observations for unclamped barium titanate single crystals where increasing thermal conductivity was observed when an electric field was applied, resulting from reduced populations of ferroelastic domain boundaries in the crystal.[10]

The polarization versus field and microdiffraction data also support the lack of a change in thermal conductivity when negative biases were applied to the membrane. The maximum field applied under negative bias was intentionally limited as an increasing loss tangent was observed, and we sought to limit the degradation of the device to allow for additional experiments. Under these applied voltage constraints, a sufficient negative bias was not subjected to the device (−100 kV/cm) to overcome the imprint. From the polarization field data, it is evident that a field in excess of −130 kV/cm would be necessary to switch the domains and observe a tuning of thermal conductivity.

Aside from the opposite sign of the thermal conductivity change in the membrane structure PZT films compared to bilayer PZT films,[17] the nature of transition is substantially different. The bilayer PZT films displayed a nearly linear dependence of the degree of thermal conductivity tuning because of the applied fields—the higher the voltage applied, the greater the change in thermal conductivity, resulting in an *analog* response of thermal conductivity with the field. The membrane structures, however, responded in a more *digital* sense, where the thermal conductivity exhibited an abrupt, discrete change at a fixed field and did not change substantially with additional voltage of the same polarity. This difference can be reconciled by considering the degree of clamping and the shape of the polarization-field response between the two PZT samples. The bilayer film, which was clamped to an underlying silicon substrate, displayed a slanted polarization response, whereas the films in the membrane structure, where the clamping was reduced, exhibited a square hysteresis loop. The polarization switching in the latter case is more abrupt and indicates that the domain structure changes over a much

smaller electric field range near the coercive field. The more slanted hysteresis loop and, consequently, gradual change of polarization with the applied field of the bilayer films result from more incremental changes to the domain structure as the field is increased and from a more analog response of thermal conductivity with the applied field. The abrupt change in polarization magnitude and thermal conductivity at the coercive field of the membrane structures also result in a lower necessary applied field to realize a large thermal conductivity change as evidenced by the bilayer films requiring nearly 500 kV/cm to realize a 12.5% change in thermal conductivity, whereas the films in the membrane structures required just 100 kV/cm to realize a 13% change.

It was also observed that while the thermal conductivity change was abrupt, other measured properties, such as membrane stiffness and domain volume fraction, displayed more gradual changes with the field. We hypothesize that the frequency-dependent phonon mean-free path spectrum in $Pb(Zr,Ti)O_3$ comprises a narrow band of relatively short lengths, similar to PbTe or PbSe where the mean-free path lengths are of the order of 3−10 nm.[50] This would mean that a small change in domain wall spacing would result in an abrupt change in the heat-carrying capability of a sizable population of short-wavelength phonons. Additional incremental increases in domain wall spacing, however, will cease to influence these phonons via this mechanism as the mean-free paths will be capped by phonon−phonon (umklapp) scattering. Therefore, while domains continue to grow, as evidenced by the diffraction data, the phonon-scattering landscape does not continue to change.

Finally, it was observed that after every application of an above- or near-coercive field dc bias, the thermal conductivity in the remanent (zero dc field) state increased relative to its prior value. This is shown in Figure 6 for both the membrane
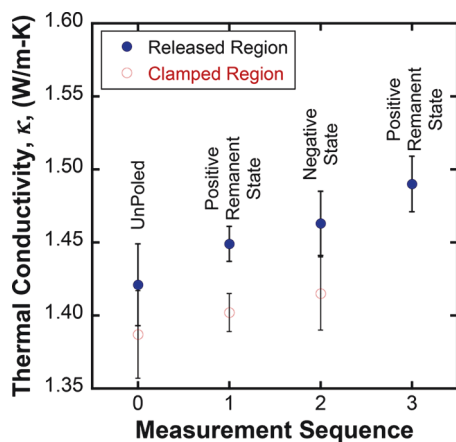

Figure 6. Thermal conductivity of PZT under zero applied bias for membrane regions (closed data points) and clamped regions (open data points) plotted as a function of measurement sequence after receiving a several minute, large bias (133 and −100 kV/cm for released regions and 133 and −133 kV/cm for clamped regions).

device and the clamped region. Note that these are the same zero bias data points plotted in Figure 2a but delineated by measurement sequence. As it has been established that the thermal conductivity is extremely sensitive to domain structure, these data indicate that the domain structure is changing irreversibly after every application of a large dc field. Subsequent several minute exposures of the high field appeared

to increase the domain wall spacing in the zero bias state, even for the clamped regions where the field-applied thermal conductivity decreased, which indicated a decrease in domain wall spacing while the field was applied. These minute changes in domain structure could be very difficult to characterize with conventional electrical probes. Thermal conductivity is therefore a very sensitive probe of the domain structure of ferroelectric thin films.

4. SUMMARY

In summary, active voltage control of thermal conductivity in a strain-released PZT thin-film device has been demonstrated with an abrupt positive change in the thermal conductivity observed. The thermal conductivity discontinuity occurred at ~100 kV/cm, which correlated with the coercive field, the onset of increased stiffness in the membrane structure, and the onset of increasing (002) domain volume fraction. The abrupt switching of thermal conductivity by a magnitude of 13% was repeatable and occurred in a time scale of less than 300 ms. This work demonstrates a new means to actively and digitally increase the thermal conductivity in a solid-phase material at room temperature with only the application of an electric field, which may enable technologies related to phononic computation and thermal management, among others.

■ AUTHOR INFORMATION

Corresponding Authors
*E-mail: phopkins@virginia.edu (P.E.H.).
*E-mail: jihlefeld@virginia.edu (J.F.I.).

ORCID ⓘ
Jon F. Ihlefeld: 0000-0003-0166-8136

Present Addresses
▽Department of Mechanical and Nuclear Engineering and Materials Research Institute, The Pennsylvania State University, University Park, PA 16802.
°General Electric, Niskayuna, NY 12309.

Notes
The authors declare no competing financial interest.

■ REFERENCES

(1) Zhu, T.; Liu, Y.; Fu, C.; Heremans, J. P.; Snyder, J. G.; Zhao, X. Compromise and Synergy in High-Efficiency Thermoelectric Materials. *Adv. Mater.* **2017**, *29*, 1605884.

(2) Lai, J.; Majumdar, A. Concurrent thermal and electrical modeling of sub-micrometer silicon devices. *J. Appl. Phys.* **1996**, *79*, 7353−7361.

(3) Grossman, E. N.; McDonald, D. G.; Sauvageau, J. E. Two-dimensional analysis of microbolometer arrays. *J. Appl. Phys.* **1990**, *68*, 5409−5414.

(4) Sun, P. C.; Wu, Y. L.; Gao, J. W.; Cheng, G. A.; Chen, G.; Zheng, R. T. Room Temperature Electrical and Thermal Switching CNT/Hexadecane Composites. *Adv. Mater.* **2013**, *25*, 4938−4943.

(5) Zheng, R.; Gao, J.; Wang, J.; Chen, G. Reversible Temperature Regulation of Electrical and Thermal Conductivity Using Liquid-Solid Phase Transitions. *Nat. Commun.* **2011**, *2*, 289.

(6) Oh, D.-W.; Ko, C.; Ramanathan, S.; Cahill, D. G. Thermal conductivity and dynamic heat capacity across the metal-insulator transition in thin film VO_2. *Appl. Phys. Lett.* **2010**, *96*, 151906.

(7) Dhara, S.; Solanki, H. S.; Pawan, A. R.; Singh, V.; Sengupta, S.; Chalke, B. A.; Dhar, A.; Gokhale, M.; Bhattacharya, A.; Deshmukh, M. M. Tunable Thermal Conductivity in Defect Engineered Nanowires at Low Temperatures. *Phys. Rev. B: Condens. Matter Mater. Phys.* **2011**, *84*, 121307.

(8) Huang, H.-T.; Lai, M.-F.; Hou, Y.-F.; Wei, Z.-H. Influence of Magnetic Domain Walls and Magnetic Field on the Thermal Conductivity of Magnetic Nanowires. *Nano Lett.* **2015**, *15*, 2773−2779.

(9) Cho, J.; Losego, M. D.; Zhang, H. G.; Kim, H.; Zuo, J.; Petrov, I.; Cahill, D. G.; Braun, P. V. Electrochemically Tunable Thermal Conductivity of Lithium Cobalt Oxide. *Nat. Commun.* **2014**, *5*, 4035.

(10) Mante, A. J. H.; Volger, J. Phonon Transport in Barium Titanate. *Phys.* **1971**, *52*, 577−604.

(11) Weilert, M. A.; Msall, M. E.; Anderson, A. C.; Wolfe, J. P. Phonon Scattering from Ferroelectric Domain Walls: Phonon Imaging in KDP. *Phys. Rev. Lett.* **1993**, *71*, 735−738.

(12) Weilert, M. A.; Msall, M. E.; Wolfe, J. P.; Anderson, A. C. Mode Dependent Scattering of Phonons by Domain Walls in Ferroelectric KDP. *Z. Phys. B: Condens. Matter* **1993**, *91*, 179−188.

(13) Li, J.; Nagaraj, B.; Liang, H.; Cao, W.; Lee, C. H.; Ramesh, R. Ultrafast Polarization Switching in Thin-Film Ferroelectrics. *Appl. Phys. Lett.* **2004**, *84*, 1174−1176.

(14) Mitsui, T.; Furuichi, J. Domain Structure of Rochelle Salt and KH_2PO_4. *Phys. Rev.* **1953**, *90*, 193−202.

(15) Donovan, B. F.; Foley, B. M.; Ihlefeld, J. F.; Maria, J.-P.; Hopkins, P. E. Spectral Phonon Scattering Effects on the Thermal Conductivity of Nano-Grained Barium Titanate. *Appl. Phys. Lett.* **2014**, *105*, 082907.

(16) Hopkins, P. E.; Adamo, C.; Ye, L.; Huey, B. D.; Lee, S. R.; Schlom, D. G.; Ihlefeld, J. F. Effects of Coherent Ferroelastic Domain Walls on the Thermal Conductivity and Kapitza Conductance in Bismuth Ferrite. *Appl. Phys. Lett.* **2013**, *102*, 121903.

(17) Ihlefeld, J. F.; Foley, B. M.; Scrymgeour, D. A.; Michael, J. R.; McKenzie, B. B.; Medlin, D. L.; Wallace, M.; Trolier-McKinstry, S.; Hopkins, P. E. Room-Temperature Voltage Tunable Phonon Thermal Conductivity via Reconfigurable Interfaces in Ferroelectric Thin Films. *Nano Lett.* **2015**, *15*, 1791−1795.

(18) Tuttle, B. A.; Garino, T. J.; Voigt, J. A.; Headley, T. J.; Dimos, D.; Eatough, M. O. Relationships between Ferroelectric 90° Domain Formation and Electrical Properties of Chemically Prepared Pb-(Zr,Ti)O$_3$ Thin Films. *Science and Technology of Electroceramic Thin Films*; Proceedings of the NATO Advanced Research Workshop, 1995; pp 117−132.

(19) Nagarajan, V.; Roytburd, A.; Stanishevsky, A.; Prasertchoung, S.; Zhao, T.; Chen, L.; Melngailis, J.; Auciello, O.; Ramesh, R. Dynamics of Ferroelastic Domains in Ferroelectric Thin Films. *Nat. Mater.* **2003**, *2*, 43−47.

(20) Griggio, F.; Jesse, S.; Kumar, A.; Ovchinnikov, O.; Kim, H.; Jackson, T. N.; Damjanovic, D.; Kalinin, S. V.; Trolier-McKinstry, S.

(21) Wallace, M.; Johnson-Wilke, R. L.; Esteves, G.; Fancher, C. M.; Wilke, R. H. T.; Jones, J. L.; Trolier-McKinstry, S. In Situ Measurement of Increased Ferroelectric/Ferroelastic Domain Wall Motion in Declamped Tetragonal Lead Zirconate Titanate Thin Films. *J. Appl. Phys.* **2015**, *117*, 054103.

Substrate Clamping Effects on Irreversible Domain Wall Dynamics in Lead Zirconate Titanate Thin Films. *Phys. Rev. Lett.* **2012**, *108*, 157604.

(22) Bernal, A.; Tselev, A.; Kalinin, S.; Bassiri-Gharb, N. Effects of Lateral and Substrate Constraint on the Piezoresponse of Ferroelectric Nanostructures. *Appl. Phys. Lett.* **2012**, *101*, 112901.

(23) Keech, R.; Ye, L.; Bosse, J. L.; Esteves, G.; Guerrier, J.; Jones, J. L.; Kuroda, M. A.; Huey, B. D.; Trolier-McKinstry, S. Declamped Piezoelectric Coefficients in Patterned 70/30 Lead Magnesium Niobate-Lead Titanate Thin Films. *Adv. Funct. Mater.* **2017**, *27*, 1605014.

(24) Anbusathaiah, V.; Kan, D.; Kartawidjaja, F. C.; Mahjoub, R.; Arredondo, M. A.; Wicks, S.; Takeuchi, I.; Wang, J.; Nagarajan, V. Labile Ferroelastic Nanodomains in Bilayered Ferroelectric Thin Films. *Adv. Mater.* **2009**, *21*, 3497−3502.

(25) Qi, Y.; Kim, J.; Nguyen, T. D.; Lisko, B.; Purohit, P. K.; McAlpine, M. C. Enhanced Piezoelectricity and Stretchability in Energy Harvesting Devices Fabricated from Buckled PZT Ribbons. *Nano Lett.* **2011**, *11*, 1331−1336.

(26) Xu, F.; Trolier-McKinstry, S.; Ren, W.; Xu, B.; Xie, Z.-L.; Hemker, K. J. Domain Wall Motion and its Contribution to the Dielectric and Piezoelectric Properties of Lead Zirconate Titanate Films. *J. Appl. Phys.* **2001**, *89*, 1336−1348.

(27) Anbusathaiah, V.; Jesse, S.; Arredondo, M. A.; Kartawidjaja, F. C.; Ovchinnikov, O. S.; Wang, J.; Kalinin, S. V.; Nagarajan, V. Ferroelastic Domain Wall Dynamics in Ferroelectric Bilayers. *Acta Mater.* **2010**, *58*, 5316−5325.

(28) Ehara, Y.; Yasui, S.; Nagata, J.; Kan, D.; Anbusathaiah, V.; Yamada, T.; Sakata, O.; Funakubo, H.; Nagarajan, V. Ultrafast Switching of Ferroelastic Nanodomains in Bilayered Ferroelectric Thin Films. *Appl. Phys. Lett.* **2011**, *99*, 182906.

(29) Ivry, Y.; Wang, N.; Chu, D.; Durkan, C. 90° Domain Dynamics and Relaxation in Thin Ferroelectric/Ferroelastic Films. *Phys. Rev. B: Condens. Matter Mater. Phys.* **2010**, *81*, 174118.

(30) Shelton, C. T.; Kotula, P. G.; Brennecka, G. L.; Lam, P. G.; Meyer, K. E.; Maria, J.-P.; Gibbons, B. J.; Ihlefeld, J. F. Chemically Homogeneous Complex Oxide Thin Films via Improved Substrate Metallization. *Adv. Funct. Mater.* **2012**, *22*, 2295−2302.

(31) Assink, R. A.; Schwartz, R. W. Proton and carbon-13 NMR investigations of lead zirconate titanate (Pb(Zr,Ti)O$_3$) thin-film precursor solutions. *Chem. Mater.* **1993**, *5*, 511−517.

(32) Hiboux, S.; Muralt, P.; Setter, N. Orientation and Composition Dependence of Piezoelectric-Dielectric Properties of Sputtered Pb(Zr$_x$,Ti$_{1-x}$)O$_3$ Thin Films. *MRS Proceedings*; Cambridge University Press: New York, USA, 1999; Vol. 596, pp 499−504.

(33) Muralt, P.; Maeder, T.; Sagalowicz, L.; Hiboux, S.; Scalese, S.; Naumovic, D.; Agostino, R. G.; Xanthopoulos, N.; Mathieu, H. J.; Patthey, L.; Bullock, E. L. Texture control of PbTiO$_3$ and Pb(Zr,Ti)O$_3$ thin films with TiO$_2$ seeding. *J. Appl. Phys.* **1998**, *83*, 3835−3841.

(34) Hopkins, P. E.; Serrano, J. R.; Phinney, L. M.; Kearney, S. P.; Grasser, T. W.; Harris, C. T. Criteria for Cross-Plane Dominated Thermal Transport in Multilayer Thin Film Systems During Modulated Laser Heating. *J. Heat Tran.* **2010**, *132*, 081302.

(35) Cahill, D. G.; Goodson, K.; Majumdar, A. Thermometry and Thermal Transport in Micro/Nanoscale Solid-State Devices and Structures. *J. Heat Tran.* **2002**, *124*, 223−241.

(36) Schmidt, A. J.; Chen, X.; Chen, G. Pulse Accumulation, Radial Heat Conduction, and Anisotropic Thermal Conductivity in Pump-Probe Transient Thermoreflectance. *Rev. Sci. Instrum.* **2008**, *79*, 114902.

(37) Gaskins, J.; Scott Barker, N.; Begley, M. R. Comprehensive Solutions for the Response of Freestanding Beams With Tensile

Residual Stress Subject to Point-Loading. *J. Appl. Mech.* **2013**, *81*, 031008.

(38) Maner, K. C.; Begley, M. R.; Oliver, W. C. Nanomechanical Testing of Circular Freestanding Polymer Films with Sub-Micron Thickness. *Acta Mater.* **2004**, *52*, 5451−5460.

(39) Komaragiri, U.; Begley, M. R.; Simmonds, J. G. The Mechanical Response of Freestanding Circular Elastic Films Under Point and Pressure Loads. *J. Appl. Mech.* **2005**, *72*, 203−212.

(40) Casset, F.; Devos, A.; Sadtler, S.; Le Louarn, A.; Emery, P.; Le Rhun, G.; Ancey, P.; Fanget, S.; Defay, E. Young Modulus and Poisson Ratio of PZT Thin Film by Picosecond Ultrasonics. *2012 IEEE International Ultrasonics Symposium*; IEEE: New York, 2012; pp 2180−2183.

(41) Yoshimura, H. N.; Molisani, A. L.; Narita, N. E.; Manholetti, J. L. A.; Cavenaghi, J. M. Mechanical Properties and Microstructure of Zinc Oxide Varistor Ceramics. *Advanced Powder Technology V*; Salgado, L., Filho, F. A., Eds.; Trans Tech Publications Ltd: Durnten-Zurich, 2006; Vol. *530−531*, pp 408−413.

(42) Munro, R. G. Elastic Moduli Data for Polycrystalline Oxide Ceramics. *In NISTIR 6853*; U.S. Dept. of Commerce, Technology Administration, National Institute of Standards and Technology: Gaithersburg, MD, 2002; Vol. SDR Database Number 30.

(43) Merker, J.; Lupton, D.; Topfer, M.; Knake, H. High Temperature Mechanical Properties of the Platinum Group Metals: Elastic Properties of Platinum, Rhodium, and Iridium and Their Alloys at High Temperatures. *Platinum Met. Rev.* **2001**, *45*, 74−82.

(44) Ehara, Y.; Yasui, S.; Oikawa, T.; Shiraishi, T.; Shimizu, T.; Tanaka, H.; Kanenko, N.; Maran, R.; Yamada, T.; Imai, Y.; Sakata, O.; Valanoor, N.; Funakubo, H. In-situ Observation of Ultrafast 90° Domain Switching Under Application of an Electric Field in (100)/(001)-Oriented Tetragonal Epitaxial $Pb(Zr_{0.4}Ti_{0.6})O_3$ Thin Films. *Sci. Rep.* **2017**, *7*, 9641.

(45) Pan, W.; Thio, C. L.; Desu, S. B. Reactive Ion Etching Damage to the Electrical Properties of Ferroelectric Thin Films. *J. Mater. Res.* **2011**, *13*, 362−367.

(46) Jang, H. W.; Baek, S. H.; Ortiz, D.; Folkman, C. M.; Eom, C. B.; Chu, Y. H.; Shafer, P.; Ramesh, R.; Vaithyanathan, V.; Schlom, D. G. Epitaxial (001) $BiFeO_3$ membranes with substantially reduced fatigue and leakage. *Appl. Phys. Lett.* **2008**, *92*, 062910.

(47) Wieder, H. H. Activation Field and Coercivity of Ferroelectric Barium Titanate. *J. Appl. Phys.* **1957**, *28*, 367−369.

(48) Chaplya, P. M.; Carman, G. P. Compression of piezoelectric ceramic at constant electric field: Energy absorption through non-180° domain-wall motion. *J. Appl. Phys.* **2002**, *92*, 1504−1510.

(49) Bassiri-Gharb, N.; Fujii, I.; Hong, E.; Trolier-McKinstry, S.; Taylor, D. V.; Damjanovic, D. Domain Wall Contributions to the Properties of Piezoelectric Thin Films. *J. Electroceram.* **2007**, *19*, 47−65.

(50) Tian, Z.; Garg, J.; Esfarjani, K.; Shiga, T.; Shiomi, J.; Chen, G. Phonon conduction in PbSe, PbTe, $PbTe_{1-x}Se_x$ from first-principles calculations. *Phys. Rev. B: Condens. Matter Mater. Phys.* **2012**, *85*, 184303.